

Article

# Fitting Type Ia Supernova Data to a Cosmological Model Based on Einstein–Newcomb–De Sitter Space

Vladimir N. Yershov 

Formerly Mullard Space Science Laboratory, University College London, Holmbury St.Mary, Dorking RH5 6NT, UK; vyershov@moniteye.co.uk

**Abstract:** Einstein–Newcomb–de Sitter (ENdS) space is de Sitter’s modification of spherical space used by Einstein in his first cosmological model paper published in 1917. The modification by de Sitter incorporated the topological identification of antipodal points in space previously proposed by Newcomb in 1877. De Sitter showed that space topologically modified in this way (called elliptical or projective space) satisfies Einstein’s field equations. De Sitter also found that in a space with constant positive curvature, spectral lines of remote galaxies would be red-shifted (called the de Sitter effect). However, de Sitter’s formulae relating distances to red shifts do not satisfy observational data. The likely reason for this mismatch is that de Sitter mainly focused on space curvature and ignored the identification of antipodal points. Herein, we demonstrate that it is this particular feature that allows an almost perfect fit of the ENdS-based cosmological model to observational data. We use 1701 sources from the type Ia supernovae data sample called *Pantheon+*, which was previously used to fit the  $\Lambda$ CDM model.  $\Lambda$ CDM and ENdS diverge in their predictions for red shifts exceeding  $z \sim 2.3$ . Since there are no available type Ia supernovae (SNe) data for higher red shifts, both models can be validated by using an additional sample of 193 gamma-ray bursts (GRBs) spanning red shifts up to  $z \sim 8$ . This validation shows that the minimum  $\chi^2$  for the SNe+GRBs sample is about 2.7% smaller for the ENdS space model than for the  $\Lambda$ CDM model.

**Keywords:** type Ia supernovae; elliptical space; wormholes; nonlocality; Schwarzschild metric; gravitational red shift; cosmological red shift



**Citation:** Yershov, V.N. Fitting Type Ia Supernova Data to a Cosmological Model Based on Einstein–Newcomb–De Sitter Space. *Universe* **2023**, *9*, 204. <https://doi.org/10.3390/universe9050204>

Academic Editor: Kazuharu Bamba

Received: 31 March 2023

Revised: 21 April 2023

Accepted: 22 April 2023

Published: 25 April 2023



**Copyright:** © 2023 by the author. Licensee MDPI, Basel, Switzerland. This article is an open access article distributed under the terms and conditions of the Creative Commons Attribution (CC BY) license (<https://creativecommons.org/licenses/by/4.0/>).

## 1. Introduction

The first cosmological model was introduced in 1917 by A. Einstein [1]. It was based on static space with constant positive curvature. At that time, Einstein was not concerned with the cosmological red-shift problem because there was no observational evidence for such a phenomenon at the time, and the universe was commonly believed to be static. Therefore, Einstein introduced to his model a fine-tuned cosmological constant to make space static.

Even so, based on Einstein’s static universe model alone, it was already possible to foresee the existence of cosmological red shift. This was described by W. de Sitter [2], who analysed various cosmological models based on positively curved three-manifolds of spherical ( $S^3$ ) and elliptical shapes, the latter having been previously studied by S. Newcomb [3]. For brevity, we use the acronym ENdS (Einstein–Newcomb–de Sitter) when referring to this particular version of de Sitter’s models.

Elliptical space (also called projective space ( $\mathbb{P}^3$ )) differs from  $S^3$  by identification of antipodal points, which is schematically shown in Figure 1 in the form of an embedding diagram, in which spherical curvature is neglected for simplicity. Two antipodal points of space are separated from each other by the maximal possible distance corresponding to the projective angle ( $\chi = \pi$ ) (the solid and dot-dashed line along the manifold in this diagram). Topological identification is indicated by the dashed line connecting two points in the perpendicular direction. According to de Sitter, elliptical space ( $\mathbb{P}^3$ ) is preferable

for modelling the physical world because when  $\mathbb{P}^3$  is projected to the Euclidean ( $\mathbb{E}^3$ ) or hyperbolic ( $\mathbb{H}^3$ ) spaces, it covers them once, whereas  $\mathbb{S}^3$  covers them twice. The projection corresponds to the coordinate transformation

$$r = R \tan \chi, \tag{1}$$

where  $R^{-2}$  is the constant positive curvature of  $\mathbb{S}^3$  or  $\mathbb{P}^3$ , and  $\chi$  is the projective angle. Locally,  $\mathbb{S}^3$  and  $\mathbb{P}^3$  are identical to  $\mathbb{E}^3$ . However, de Sitter noted that since velocity and energy are related to different reference frames, they change when observed from one or another reference frame. The time component of the elliptical space metric is

$$g_{tt} = \cos^2 \chi. \tag{2}$$

Therefore, from the point of view of a remote observer, all physical processes slow down, including chemical and atomic reactions, which leads to the reduced frequencies of electromagnetic waves emitted in these reactions. This time-dilatation effect (called the de Sitter effect) was regarded by E. Hubble as one of the main possible physical mechanisms explaining the distance–red shift relationship [4].

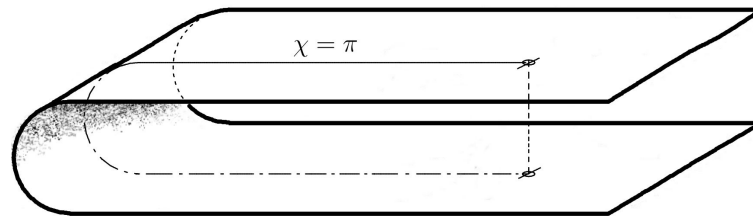


**Figure 1.** Embedding diagram of Einstein–Newcomb–de Sitter elliptical space with two antipodal points topologically identified (the dashed line). The radius of curvature ( $R$ ) is neglected in this plot for simplicity. The distance between two antipodal points is measured along the spatial coordinate (thin solid and dot-dashed line) by the projective angle ( $\chi$ ), which is equal to  $\pi$  for the maximal possible separation in the elliptical space.

An alternative interpretation of the distance–red shift relationship due to space expansion was widely debated by many authors, including A. Friedmann [5], G. Lemaître [6], H.P. Robertson [7] and A. G. Walker [8] (FLRW), whose approach became a basis for the standard FRLW cosmological model. The 1998 discovery of type Ia SNe excessive dimming at  $z \simeq 1$  [9–11] was interpreted as evidence in favour of dark energy—repulsive gravity or the  $\Lambda$  term in Einstein’s equations, which was incorporated into the standard cosmological model, together with cold dark matter (CDM) detected via its gravitational effects. Among other expanding universe models, the standard  $\Lambda$ CDM cosmological model is the best to fit observational data, including the accurately measured distance moduli of type Ia supernovae and the fluctuations of the cosmic microwave background (CMB).

In recent years, the standard cosmological model has been subject to some problems. For example, extremely remote galaxies were found to host very high-mass supermassive black holes, with not enough time for their formation since the beginning of the universe [12]. Galaxies were also discovered whose sizes and surface brightness contradicted the predictions of  $\Lambda$ CDM [13]. More recently, observations made using the James Webb Space Telescope have demonstrated that there are many well-evolved galaxies with red shifts ( $z > 15$ ) that must have been formed in an impossibly short time span of  $\sim 230$  Myr available since the beginning of the universe according to  $\Lambda$ CDM (see a review by N. Lovyagin [14] and references therein). Static cosmological models provide much more time for the evolution of those galaxies, which would explain the unexpected JWST results.

All this suggests that the old debate on the nature of the cosmological red shift needs to be revived. This debate has lasted since the 1930s [15–17] through the 1970s–1990s [18–21], continuing to very recent years [22,23]. Herein, we contribute to this debate but without

exploring the de Sitter effect in its original form [2], or the Zwicky’s photon-energy dissipation mechanism [15], as neither matches the modern standard-candle data based on the type Ia supernovae distance moduli.

Instead, we focus on a different aspect of ENdS elliptical space, namely the topological identification of antipodal points. This aspect was neglected by de Sitter when he associated distances with red shifts in his theory, likely due to the oversight that de Sitter’s formulae, (1) and (2), do not match observations.

In order to relate red shifts to distances in the elliptical space, the mathematical concept of identical antipodal points needs to be interpreted in the form of a physical model. We propose such an interpretation in the next section. In Section 2.2, we derive a formalism relating the luminosity distances of remote sources with their cosmological red shifts, which is needed to obtain parameter values for our model using accurately calibrated observational data of type Ia supernovae (Section 2.3). In Section 3, we compare the theoretical predictions of the  $\Lambda$ CDM and ENdS models with the distance moduli based on type Ia supernova data from the *Pantheon+* sample. In Section 4, we validate our model via an external  $\chi^2$  criterion for red shifts exceeding  $z \simeq 2.3$  using gamma-ray burst (GRB) distance moduli provided by L. Amati et al. [24].

## 2. Materials and Methods

### 2.1. Physical Interpretation of Identified Antipodal Points

The topological identification of antipodal points of a manifold is a mathematical abstraction. In order to interpret this in terms of physics, we would need to find a physical object, preferably one described in a generally relativistic way, which allows widely separated points of space to be connected. Such an object was found and described in 1935 within the framework of the theory of general relativity by the very author of this theory [25]. It is called an Einstein–Rosen bridge or, more frequently, a “wormhole” because it can connect two different spaces (universes).

Later on, it was found that wormholes may connect widely separated regions of the same space, which was viewed as a possibility for interstellar travel [26]. Thus, wormholes can also connect antipodal points of ENdS space, which is what we require. This is schematically shown in Figure 2 in the form of an embedding diagram, where the topological connection previously indicated as a dashed line in Figure 1 is now replaced with a wormhole’s throat. In Figure 2, the observer (*o*) and the observed source (*s*) are at distances of  $r_o$  and  $r_s$ , respectively, from the far end of the wormhole’s throat, where  $r_g$  is the wormhole’s gravitational radius. The source is at a distance of  $d = r_o - r_s$  from the observer, and we need to relate this distance to the observed red shift ( $z$ ) of the source (*s*) in order to compare our model with observations.

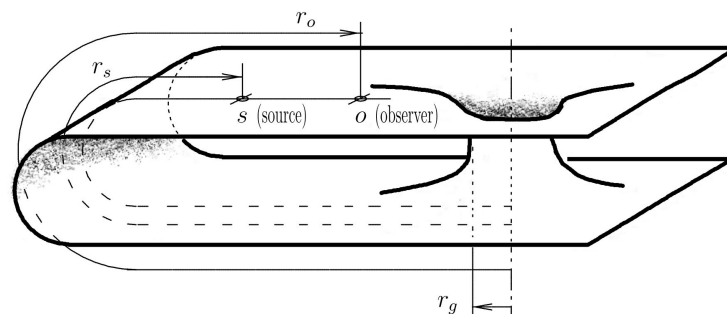


**Figure 2.** Embedding diagram depicting a possible physical realisation of the topological connection between two distant (antipodal) regions of space via a wormhole structure. Here,  $r_o$  and  $r_s$  are distances of the observer (*o*) and source (*s*) from the wormhole’s far throat, opposite to the near throat in the vicinity of the observer; and  $r_g$  is the gravitational radius of the wormhole.

M.S. Morris, K.S. Thorne and U. Yurtsever highlighted [27] that wormhole creation is accompanied by extremely large space-time curvature, which corresponds to microscopic struc-

tures on a scale length of the order of the Planck–Wheeler length,  $\sqrt{G\hbar/c^3} = 1.3 \times 10^{-33}$  cm. Therefore, in principle, wormholes can be microscopic. There might be an arbitrarily large number ( $n$ ) of microscopic wormholes, and when  $n \rightarrow \infty$ , physical space becomes approximately equivalent to its mathematical idealisation, called elliptical space.

The fact that two sides of the wormhole’s throat can be located at a very large distance from each other can be (and is) used to solve the Einstein–Podolsky–Rosen (EPR) paradox [28] and to explain the phenomenon of quantum entanglement of subatomic particles separated by large distances (see, e.g., [29]).

Einstein referred to the possibility of quantum entanglement as to a “spooky action at distance” [30]. However, surprisingly, it is his own wormhole theory [25] that provides a solution to the quantum entanglement and nonlocality puzzle<sup>1</sup>. This implies that quantum mechanics, in order to be consistent, require general relativity, which is not a welcome idea to most modern physicists. However, the matter stands.

Herein, we do not discuss the possibility of solving the EPR paradox using the connectivity between distant regions of space via wormholes. Instead, we focus on another aspect of this nonlocal connectivity, namely the possibility of perceiving the event horizons of local microscopic wormholes (near the observer) as horizons in the far distance from the observer, as these horizons have an effect on both the source and the observer remote from the far-throats of the same wormholes.

These remote horizons of local microscopic wormholes are spherically symmetric around the observer. This follows from the topology of the elliptical space. For example, when looking at the near throat of a microscopic wormhole, the observer localises it within a very narrow solid angle (a zero-aperture solid angle in the case of the mathematical elliptical space). However, when the observer looks at the far throat of the same microscopic wormhole, the solid angle spans  $4\pi$  steradians (a sphere around the observer), even in the case of an ideal elliptical space when the far throat of the wormhole at  $\chi = \pi$  is point-like.

As the remote horizons are at extremely large distances from the observer, their deviations from spherical symmetry due to different locations of neighbouring points around the observer are negligible. Furthermore, the average global collective horizon around any point of ENdS space is practically ideally spherically symmetric, making all points of this space equivalent to each other from the observer’s perspective.

As with any Schwarzschild event horizon, there is an associated gravitational red shift, which is calculable when we know the distances from the horizon to the source and to the observer. Thus, in this particular setup, the observed cosmological red shift is gravitational in nature. However, in principle, this gravitational red shift can be mixed with the red shift caused by the changing scale factor of the FLRW metric, as the concept of space expansion can equally be applied to ENdS space. Therefore, the resulting cosmological red shift might be a mix of the gravitational red shift with the red shift caused by a changing scaling factor. We shall discuss this option later elsewhere.

### 2.2. Red Shift–Distance Relationship

Consistent with ENdS, we adopt the Schwarzschild metric related to the global remote horizon. In our setup (Figure 2), we include unknown distances ( $r_s, r_o$ ), the source-to-observer distance ( $d = r_o - r_s$ ) and the unknown gravitational radius ( $r_g$ ). Both the source and observer are within the Schwarzschild metric, which corresponds to the following spacetime interval in spherical coordinates ( $r, \theta, \phi$ ):

$$ds^2 = g_{tt}c^2dt^2 - g_{rr}dr^2 - r^2(d\theta^2 + \sin^2\theta d\phi^2), \tag{3}$$

where  $g_{tt} = 1 - \frac{r_g}{r}$  and  $g_{rr} = g_{tt}^{-1}$ . The source’s red shift with respect to the observer is

$$z = \sqrt{g_{tt}^o/g_{tt}^s} - 1, \tag{4}$$

or, if we define  $r_g := 1$  as the distance unit,

$$(1+z)^2 = (1-r_o^{-1})(1-r_s^{-1})^{-1}. \tag{5}$$

Then, the source-to-observer distance reads

$$d(z) = r_o - [1 - (1 - r_o^{-1})(1+z)^{-2}]^{-1} \text{ [in units of } r_g], \tag{6}$$

which has to be multiplied by the scaling factor  $((1+z)^2)$  in order to obtain the luminosity distance

$$d_L(z) = \left\{ r_o - [1 - (1 - r_o^{-1})(1+z)^{-2}]^{-1} \right\} (1+z)^2, \tag{7}$$

with one of the  $(1+z)$  factors accounting for the decrease in the number of incoming photons due to time dilatation in the Schwarzschild metric (the  $g_{tt}$  metric coefficient) and another accounting for the photon path distortion (the  $g_{rr}$  metric coefficient). Equation (7) is the required red shift–luminosity relationship, permitting us to compare the ENdS-based model with observational data.

### 2.3. Comparison with Observations

In order to compare the theoretical luminosity distances with observational data (e.g., distance moduli of the type Ia supernovae), the distances need to be scaled and converted into magnitude values comparable with the observed source magnitudes.

For our comparison, we use the well-calibrated sample of 1701 type Ia SNe called *Pantheon+* [32,33]. The uncertainty of the parameters of the standard  $\Lambda$ CDM cosmological model were recently substantially reduced using this *Pantheon+* sample [34]. For example, the uncertainty in the  $H_0$  parameter was reduced to  $\pm 1$  km/s/Mpc.

Although the  $\Lambda$ CDM model was previously fitted to the *Pantheon+* sample by D. Brout et al. [33], we repeat that fit here to ensure that our calculation algorithms, when applied to both  $\Lambda$ CDM and ENdS, remain the same in order to consistently intercompare these two models<sup>2</sup>.

Starting with the  $\Lambda$ CDM model, the luminosity distance in this model is calculate as a function of red shift ( $z$ ) from

$$D_L(z) = D_A(z)(1+z)^2, \tag{8}$$

where the scaling factor  $((1+z)^2)$  is the same as in Equation (7), and  $D_A$  is the angular diameter distance:

$$D_A(z) = \frac{c}{H_0} \frac{1}{1+z} \int_0^z \frac{dz'}{\sqrt{1 + \Omega_M[(1+z')^3 - 1]}}, \tag{9}$$

as calculated for a flat cosmology ( $\Omega_k = 0$ ). On the other hand, the luminosity distance is defined as the relationship between the bolometric flux and luminosity of a source, which is encoded in the source distance moduli provided by the *Pantheon+* sample. If  $D_L$  is expressed in Mpc, the distance modulus is

$$\mu_{\Lambda\text{CDM}} = 5 \log D_L + 25. \tag{10}$$

### 3. Results

By fitting the theoretical values (10) to the observationally determined distance moduli of type Ia supernovae, we can find the values of the  $\Lambda$ CDM parameters. In the flat  $\Lambda$ CDM, there are two free parameters— $H_0$  and  $\Omega_M$ —and a fixed parameter,  $\Omega_\Lambda = 1 - \Omega_M$ . The fit can be achieved by minimising Pearson’s  $\chi^2$  [33]:

$$\chi^2 = \Delta \mathbf{D}^T \mathbf{C}^{-1} \Delta \mathbf{D}, \tag{11}$$

where  $C$  is the covariance matrix, and  $\Delta\mathbf{D}$  is the vector of SN distance–modulus residuals

$$\Delta\mathbf{D}_i = \mu_{\Lambda\text{CDM}}(z_i) - \mu_i, \tag{12}$$

the length of which is  $N = 1701$  for the *Pantheon+* sample.

Since here, we are only interested in comparing the goodness of fit of two different cosmological models, we do not need to reach out for the correct cosmological parameters via these fits. Thus, we can use a simplified statistic

$$\chi^2 = (\text{diag } C^T \Delta\mathbf{D})^2 = \sum_{i=1}^N \frac{\Delta\mathbf{D}_i^2}{\sigma_{\mu_i}^2}, \tag{13}$$

where  $\sigma_{\mu_i}^2$  are the uncertainties of  $\mu_i$  as determined from the diagonal of the covariance matrix (see, e.g., [36], § IIIc for theoretical work or [37] for practical examples of using (13) and the *Pantheon* sample [38] for comparison of various cosmological models between each other). For our comparison, we use  $\mu_{\text{SH0ES}}$  from [33], which are the corrected distance moduli where fiducial type Ia SNe magnitudes ( $M$ ) were determined from SH0ES 2022 Cepheid host absolute distances [34]. This minimisation of  $\chi^2$  gives

$$\begin{aligned} H_0 &= 72.429_{-0.109}^{+0.116} \text{ [km/s/Mpc]}; \\ \Omega_M &= 0.389_{-0.007}^{+0.010}, \end{aligned} \tag{14}$$

which differ, as expected, from those based on the full covariance matrix ( $H_0 = 73.6 \pm 1.1$  [km/s/Mpc];  $\Omega_M = 0.334 \pm 0.018$  [33]). This is acceptable, as we are interested in the goodness of fit characterised by the minimal value

$$\chi_{\Lambda\text{CDM}}^2 = 881.15. \tag{15}$$

Minimisation is achieved by the global descent method with consecutive iterations, and the confidence limits in (14) are estimated by using the calculated parameter values corresponding to Pearson’s probability of 68.3% divided by the square root of the number of degrees of freedom ( $\sqrt{N - n_p}$ ), where the number of free parameters is  $n_p = 2$ .

In the case of ENdS, besides its free parameter ( $r_o$ ), the expression (10) requires an extra free parameter, such as  $s_g$  (a scaling factor), in order to match the theoretical  $\mu_{\text{ENdS}}$  with the observationally determined  $\mu$  from the type Ia SNe:

$$\mu_{\text{ENdS}} = 5 \log(s_g d_L) + 25, \tag{16}$$

because  $d_L$  is expressed in units of  $r_g$ , and we need to scale it to Mpc. Thus, the ENdS model, like the flat  $\Lambda\text{CDM}$ , also has two free parameters, the  $\chi^2$ -minimised values of which are

$$\begin{aligned} r_o - 1 &= (9.91_{-0.01}^{+0.02}) \cdot 10^{-8}; \\ s_g &= (2.13_{-0.13}^{+0.14}) \cdot 10^{10} \text{ [Mpc]}, \end{aligned} \tag{17}$$

with the minimal  $\chi_{\text{ENdS}}^2 = 887.56$ .

The results of these two  $\chi^2$  fits are graphically presented in Figure 3, where the distance moduli ( $\mu$ ) from the type Ia SNe *Pantheon+* sample are plotted as red points, and the minimum  $\chi^2$ -fitted theoretical curves for the flat  $\Lambda\text{CDM}$  model and the ENdS model are plotted with solid and dashed curves, respectively.

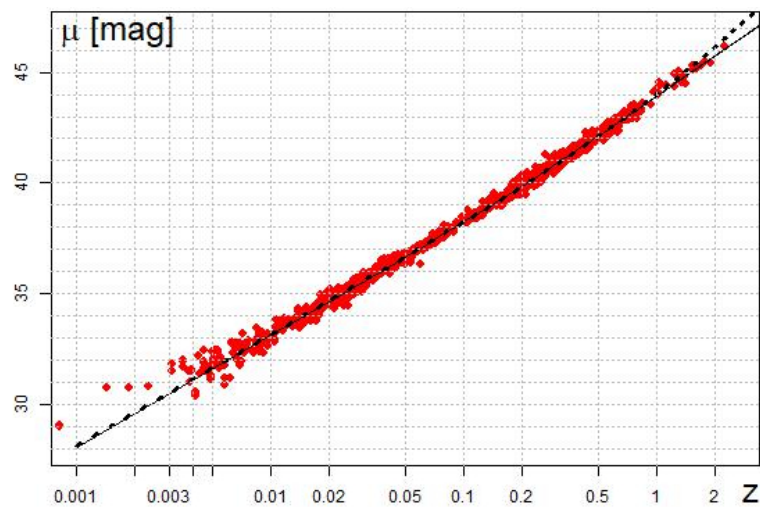


**Figure 3.** Distance moduli ( $\mu$ ) from the type Ia SNe *Pantheon+* sample (red points) as a function of red shift ( $z$ ), with the minimal  $\chi^2$ -fitted theoretical curves for the flat  $\Lambda$ CDM model (thin solid curve) and the ENdS model (dashed curve).

#### 4. Discussion

##### 4.1. Validation Using a Gamma-Ray Burst Sample

By comparing the minimal values ( $\chi^2_{\Lambda\text{CDM}} = 881.15$  and  $\chi^2_{\text{ENdS}} = 887.56$ ), we conclude that, according to observational evidence (the type Ia SNe distance moduli), both the  $\Lambda$ CDM and ENdS cosmological models compete on an equal footing with respect to the prediction of distance moduli.

We see that within the red-shift range of  $0 < z < 0.7$ , the two models are practically identical. However, for larger red shifts, the ENdS model predicts slightly larger distance moduli (fainter SNe) than those expected within the  $\Lambda$ CDM framework (see the upper-right corner of Figure 3).

The difference between the model predictions within the red-shift range of  $1 < z < 2$  is not significant (a fraction of magnitude). On the other hand, the small number of available SNe within this red-shift range and the scatter of their magnitudes do not allow for confident selection one model over the other.

For a robust comparison of these two models, we would need accurately calibrated type Ia SNe with red shifts of  $z > 3$ . Unfortunately, they have not yet been discovered. However, they are expected to be discovered in a few years by the James Webb Space Telescope (JWST). Should the future newly discovered SNe with  $z > 3$  be fainter than what is expected in  $\Lambda$ CDM cosmology, then our cosmological model based on Einstein–Newcomb–de Sitter space would be robustly confirmed.

The 1998 discovery of type Ia SNe excessive dimming at  $z \simeq 1$  [9–11] was interpreted as evidence in favour of dark energy (repulsive gravity or the  $\Lambda$  term in Einstein’s equations). In physics, dark energy is an unknown entity, and it can only be viably physically interpreted in terms of vacuum energy. Experimental evidence from particle physics suggests that the vacuum energy density (due to quantum fluctuations) must be large enough that it is discrepant by the order of  $10^{120}$  from what is currently deduced from type Ia SNe observations.

In contrast, the competing model based on ENdS space discussed here is based on the experimentally observed effect of gravitational red shift. In addition, the ENdS model prediction can be appropriately validated in the near future via the expected aforementioned JWST discoveries.

As we cannot yet do so due to the lack of standard candle data for  $z > 3$ , we can get a hint of what these data might be by using a proxy for standard candle data in the form of gamma-ray burst distance moduli ( $\mu_{\text{GRB}}$ ) obtained via the Amati relation [24]. These GRB distance moduli ( $\mu_{\text{GRB}}$ ) are extremely noisy in comparison with the distance moduli ( $\mu$ )

of the type Ia SNe, including a low-red shift systematic bias of  $\mu_{\text{GRB}}$ . We calculated this systematic bias to be  $+0.258$  (mag) by minimising  $\chi^2$  for the 27  $\mu_{\text{GRB}}$  values for  $z < 0.7$  (as the  $\Lambda$ CDM and ENdS models are identical within this red-shift range). The distance moduli of both type Ia SNe (red points) and GRBs (blue points) are plotted in Figure 4, with the GRB red shifts projected to  $z \simeq 8$ . As in the previous plot, the  $\Lambda$ CDM-based theoretical distance moduli are indicated by a thin, solid curve, and the ENdS-based distance moduli are indicated by a thicker dashed curve.

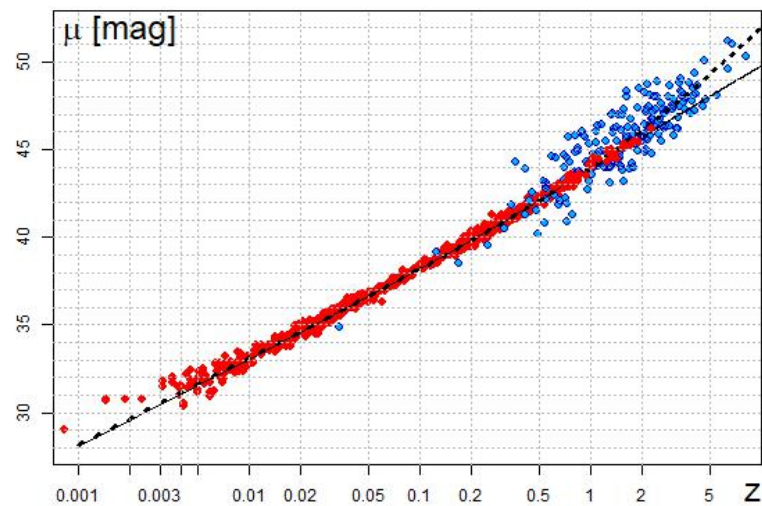


**Figure 4.** Distance moduli  $\mu$  from the *Pantheon+* type Ia SNe sample (red points), together with the distance moduli from the GRB sample (blue points) calibrated using the Amati relation. The thin, solid and thick, dashed curves indicate the minimum  $\chi^2$ -fitted theoretical curves for the flat  $\Lambda$ CDM and ENdS models, respectively.

A large sample of quasars spanning approximately the same red-shift range as GRBs is also available [39]. This sample is thought to be useful as yet another proxy for cosmological standard candles. However, the sample of quasars is strongly affected by the observational selection effect for  $z > 3$ , as found by Raikov, Lovyagin & Yershov [40]. This means that this sample cannot be used for robust validation of cosmological models. Some other authors, e.g., M. López-Corredoira [41] and N. Khadka & B. Ratra [42], arrived at the same conclusion, which is why we do not use quasars in our study.

#### 4.2. Experimental Challenges of Static and Dynamic Cosmological Models

Our analysis favours a static rather than expanding cosmological model. Static models were largely superseded by the standard cosmological model of the expanding universe because it appeared to explain many observations in an elegant way, including the formation of light elements, the cosmic microwave background and the power spectrum of matter overdensities in the local universe. The standard  $\Lambda$ CDM cosmology has therefore been almost universally adopted because of its strength in explaining observational evidence.

However, the same observational evidence has, in the past, also been used to support static universe models. As we previously mentioned in Section 1, the cosmological red shift was predicted by de Sitter for Einstein's static model well before such a phenomenon was experimentally discovered [2]. A thermalised background radiation with  $T = 3$  K (CMB) for a static universe was predicted in 1926 by A.S. Eddington [43], and with  $T = 2.8$  K by W. Nernst in 1937 [44]. These predictions were also made well before G. Gamow's CMB prediction in 1953 for the expanding universe [45]. Further detailed explanations of CMB properties in the framework of a static universe model were made by several authors, including Yu. Baryshev [46], M. Cirkovic [23] and others. As for the temperature (energy) of CMB photons arriving at the observer from remote distances, it scales with red shift in ENdS space in exactly the same way as in expanding universe models,

$$T(z) = T_0(1 + z), \quad (18)$$

where  $T_0 \approx 2.7$  K. It follows from the fact that both models reproduce the Hubble law, i.e., photons arriving from further away (including remote background photons) have reduced energies compared with the energies of photons emitted nearer to the observer. The possibility that the cosmic background has a local origin in static universe models is confidently excluded by measurements of excitation lines in absorption features of quasar spectra (for example, see [47]) or by measuring the imprint of galaxy clusters on the cosmic background via the Sunyaev–Zeldovich effect, as in [48]. However, for a cosmic background of a distant origin, the temperature–red shift relation in static universe models follows Equation (18). As mentioned above in Section 2.1, ENdS space evolves over time. Therefore, in contrast with any purely static universe model, the origin of the remote cosmic background in the model based on ENdS space can include an evolutionary component similar to expanding universe models.

The abundances of light elements in a static universe were explained by G.R. Burbidge and F. Hoyle [18,19], R. Salvaterra and A. Ferrara [49] and others. However, there are some unresolved issues for static universe models. For example, according to the standard cosmological model, deuterium ( $^2\text{H}$ ) was created exclusively during the Big Bang nucleosynthesis stage, after which it cannot be produced and can only be destroyed in stars [50]. Therefore, its observed abundance is gradually diminishing. Similarly, lithium ( $^7\text{Li}$ ) is also regarded as having been produced during the Big Bang nucleosynthesis. However, observations suggest its continuous enrichment due to cosmic-ray spallation [51].

There are other elements (e.g., beryllium and boron) that cannot be produced in stars. Their existence can be explained by a solution in the form of cosmic-ray spallation/fusion reactions [52]. This solution has been extensively studied and discussed by many authors, e.g., [53–55]. It opens an alternative way to model light element formation, which is required by static and semistatic cosmological models [19]. This mechanism also provides the possibility of producing  $^2\text{H}$ , as well as of replenishment of  $^1\text{H}$  that has been burned in nuclear reactions in stars. Since the energies of cosmic rays can be as high as  $10^{19}$  eV, they can produce spallation fragments, even from  $^4\text{He}$  [56].  $^4\text{He}$  spallation processes can also involve highly energetic neutrinos [57]. Reactions of this kind are absolutely real, as they are regularly observed in laboratory experiments [58].

Other alternatives to Big Bang nucleosynthesis are the synthesis of light elements in massive objects within the nuclear regions of galaxies [18] and the creation of practically the whole periodic table of the elements in extreme processes involving relativistic compact objects, e.g., neutron stars [59,60]. As all the abovementioned alternatives are extensively discussed in literature, we do not need any deeper discussion here.

However, there is one issue that does require attention when considering a static universe model, which is the question of cosmic structure formation, which is resolved by the  $\Lambda$ CDM model via quantum fluctuations during the universe’s inflation stage and by baryonic acoustic oscillations in the early universe. Overdensities are then modelled by performing perturbative expansions with respect to the background FLRW geometry.

A.S. Eddington [61] demonstrated that homogeneous and isotropic perturbations cause Einstein’s static universe to be unstable, as a result of which Einstein abandoned his static cosmological model in 1931. Much later, N. Rosen proved the opposite—that Einstein’s static model was, in fact, stable [62]. This opened up the question as to whether the structure formation issue could be resolved in static universe models.

While discussing the observational challenges for static universe models, it would be unfair to ignore the problems accumulated in the past decade for the  $\Lambda$ CDM model. First, it is worth mentioning that the standard Big Bang nucleosynthesis theory is not without serious problems [63–65]. Secondly, four years ago, the Hubble constant tension issue became so acute within the standard cosmology framework, which was regarded as a crisis in modern cosmology [66].

Despite the successes of  $\Lambda$ CDM's perturbative approach to correctly predict structure-formation parameters, this approach is still challenged by the fact that on scales below 100 Mpc, the matter distribution in the universe is extremely inhomogeneous. This problem was recently alleviated by considering quasistatic models containing black hole lattices [67]. Structure formation in such models is quite complicated, but this provides a prospect for solving the structure-formation issue in static universe models, especially in those based on black holes or wormholes, such as the model discussed here.

For simplicity, herein, we discussed a static version of ENdS space. However, mentioned above in Section 2.1, the concept of space expansion/contraction can equally be applied to ENdS space. Such a mixed model needs a third free parameter, which would result in the model's slightly better fit to the *Pantheon+* SNe data. This is a work in progress, and we shall discuss it in a separate paper. However, we can already note that mixed ENdS space allows for the exploitation of the existing structure-formation and light-element-synthesis formalisms that are in use for expanding universe models.

In 2012, we found that the CMB data obtained by the Wilkinson Microwave Anisotropy Probe were contaminated by irreducible distant (intergalactic) foreground [68]. That contamination was later confirmed to persist in the *Planck* space mission measurements [69,70]. We also found that the inhomogeneities in the *Planck* CMB maps are fractal [71], which is consistent with the well-known fractal distribution of matter in the universe [72–74].

There is statistical evidence that matter overdensities and underdensities imprint on the CMB as hot and cold spots [75,76]. For example, the CMB cold spot, which is inexplicable within the  $\Lambda$ CDM framework, was found to be physically related to the Eridanus supervoid [77,78]. These results support Eddington's idea that CMB radiation could be either partially or entirely explained as thermalised radiation from matter.

Since CMB data contamination is caused by a foreground whose influence is currently impossible to take into account, it is highly likely that the CMB-derived  $\Lambda$ CDM cosmological parameters cannot be trusted.

Recently, JWST observations of highly red-shifted galaxies [79,80] have shown them to be similar in appearance to the fully developed galaxies found in the late universe, despite their impossibly short ages as calculated using  $\Lambda$ CDM. This inconsistency casts doubt on one of the foundational pillars of the standard cosmological model, which is accurate prediction of geometrical and evolutionary structure.

In turn, this fact leads us to question whether the whole bulk of observational evidence supporting  $\Lambda$ CDM is, in fact, untrustworthy. It is this observational evidence that became the main reason for building the alternative cosmological model discussed here.

## 5. Conclusions

The comparison between the standard  $\Lambda$ CDM cosmological model and the cosmological model proposed here demonstrates that these two models are practically identical in terms of their predictions for the distance moduli of the available standard candles (type Ia SNe) within the red-shift range of  $0 < z < 2.3$ .

For higher red shifts, the model based on ENdS space predicts longer-distance moduli (fainter type Ia SNe) than those calculated within the framework of the standard  $\Lambda$ CDM cosmological model. This theoretical prediction can be experimentally verified in the future, as new discoveries of type Ia SNe with  $z \simeq 3$  are expected within a few years by the JWST.

**Funding:** This research received no external funding.

**Institutional Review Board Statement:** Institutional ethical review and approval are not applicable to this study, as it does not involve animals or humans.

**Informed Consent Statement:** Not applicable.

**Data Availability Statement:** The data used to prepare this manuscript are available at <https://pantheonplush0es.github.io> (accessed on 24 April 2023) and in Table 1 from [24].

**Acknowledgments:** The author made use of the following archives for this research: (1) The *Pantheon+* type Ia supernova distance moduli from [32–34]. (2) The Gamma-ray burst distance moduli prepared by [24]. The author acknowledges the use of the R software package developed by Andrew Harris and available at [github.com/cran/cosmoFns](https://github.com/cran/cosmoFns) (accessed on 24 April 2023). I would like to thank Paul Kuin, Leslie Morrison, Alice Breeveld, and Mat Page for useful discussions on the matters investigated in this paper. I am also grateful to two anonymous reviewers who drew my attention to some missing formulae and suggested highlighting various important points in the Discussion section.

**Conflicts of Interest:** The author declares no conflict of interest.

### Abbreviations

The following abbreviations are used in this manuscript:

CMB	Cosmic microwave background (radiation)
ENdS	Einstein–Newcomb–de Sitter (space)
EPR	Einstein–Podolsky–Rosen (paradox)
FLRW	Friedmann–Lemaître–Robertson–Walker (metric)
GRB	Gamma-ray burst
JWST	James Webb Space Telescope
$\Lambda$ CDM	Lambda cold–dark matter (cosmological model)
SN	supernova.

### Notes

- <sup>1</sup> In fact, this is the only viable way of understanding what matter is and what particles of matter are made of: “there is nothing in the world except empty curved space” [31]. It is also a way of answering the question as to the origin of particle species and the pattern of three generations of fundamental fermions. These are incorporated into the Standard Model of particle physics as something given to us by nature, setting aside the question, “why do we have this particular set of fundamental particles and not something else?”. This is a related but different question, discussed by the author elsewhere.
- <sup>2</sup> There might be small differences in algorithms and software used by different research groups, so our results might also be slightly different from other previously published results. We conduct our calculations here using the R package *cosmoFns* [35] and the formulae presented above.

### References

1. Einstein, A. Kosmologische betrachtungen zur allgemeinen Relativitätstheorie. *Sitz. Preuss. Akad. Wiss Phys.* **1917**, *VL*, 142–152.
2. de Sitter, W. On Einstein’s theory of gravitation, and its astronomical consequences. Third paper. *Mon. Not. R. Astron. Soc.* **1917**, *78*, 3–28. [[CrossRef](#)]
3. Newcomb, S. Elementary theorems relating to the geometry of a space of three dimensions and of uniform positive curvature in the fourth dimension. *J. Für Die Reine Und Angew. Math.* **1877**, *LXXXIII*, 293–299.
4. Hubble, E. A relation between distance and radial velocity among extragalactic nebulae. *Proc. Natl. Acad. Sci. USA* **1929**, *15*, 168–173. [[CrossRef](#)]
5. Friedmann, A. Über die Krümmung des Raumes. *Z. Phys. A* **1922**, *10*, 377–386. [[CrossRef](#)]
6. Lemaître, G. Un univers homogène de masse constante et de rayon croissant rendant compte de la vitesse radiale des nébuleuses extra-galactiques. *Ann. Soc. Sci. Brux. A* **1927**, *47*, 49–59.
7. Robertson, H.P. Kinematics and world structure. *Astrophys. J.* **1935**, *82*, 284–301. [[CrossRef](#)]
8. Walker, A.G. On Milne’s theory of world-structure. *Proc. Lond. Math. Soc. Ser. 2* **1937**, *42*, 90–127. [[CrossRef](#)]
9. Riess, A.G.; Filippenko, A.V.; Challis, P.; Clocchiatti, A.; Diercks, A.; Garnavich, P.M.; Gillil, R.L.; Hogan, C.J.; Jha, S.; Kirshner, R.P.; et al. Observational evidence from supernovae for an accelerating Universe and cosmological constant. *Astron. J.* **1998**, *116*, 1009–1038. [[CrossRef](#)]
10. Schmidt, B.P.; Suntzeff, N.B.; Phillips, M.M.; Schommer, R.A.; Clocchiatti, A.; Kirshner, R.P.; Garnavich, P.; Challis, P.; Leibundgut, B.R.; Spyromilio, J.; et al. The high-*z* supernovae search: Measuring cosmic deceleration and global. *Astrophys. J.* **1998**, *507*, 46–63. [[CrossRef](#)]
11. Perlmutter, S.; Aldering, G.; Goldhaber, G.; Knop, R.A.; Nugent, P.; Castro, P.G.; Deustua, S.; Fabbro, S.; Goobar, A.; Groom, D.E.; et al. Measurement of  $\Omega$  and  $\Lambda$  from 42 high-redshift supernovae. *Astrophys. J.* **1999**, *517*, 565–586. [[CrossRef](#)]
12. Dolgov, A.D. Massive and supermassive black holes in the contemporary and early Universe and problems in cosmology and astrophysics. *Phys. Uspekhi* **2018**, *61*, 115–132. [[CrossRef](#)]
13. Lerner, E.J. Observations contradict galaxy size and surface brightness predictions that are based on the expanding universe hypothesis. *Mon. Not. R. Astron. Soc.* **2018**, *477*, 3185–3196. [[CrossRef](#)]

14. Lovyagin, N.; Raikov, A.; Yershov, V.; Lovyagin, Y. Cosmological model tests with JWST. *Galaxies* **2022**, *10*, 108. [[CrossRef](#)]
15. Zwicky, F. On the redshifts of spectral lines through interstellar space. *Proc. Natl. Acad. Sci. USA* **1929**, *15*, 773–779. [[CrossRef](#)]
16. Tolman, R.C. On the estimation of distances in a curved universe with a non-static line element. *Proc. Nat. Acad. Sci. USA* **1930**, *16*, 511–520. [[CrossRef](#)] [[PubMed](#)]
17. Hubble, E.; Tolman, R.C. Two methods of investigating the nature of the nebular redshift. *Astrophys. J.* **1935**, *82*, 302–337. [[CrossRef](#)]
18. Burbidge, G.R. Was there really a Big Bang? *Nature* **1971**, *233*, 36–40. [[CrossRef](#)] [[PubMed](#)]
19. Burbidge, G.R.; Hoyle, F. The origin of helium and the other light elements. *Astrophys. J.* **1998**, *509*, L1–L3. [[CrossRef](#)]
20. Baryshev, Y. The hierarchical structure of metagalaxy a review of problems. *Rep. Space Astrophys. Obs. Russ. Acad. Sci.* **1981**, *14*, 24–43.
21. Troitskij, V.S. A static model of the universe. *Astrophys. Space Sci.* **1995**, *229*, 89–104. [[CrossRef](#)]
22. Baryshev, Y.; Teerikorpi, P. *Fundamental Questions of Practical Cosmology*; Springer: Dordrecht, The Netherlands, 2012; p. 332.
23. Cirkovic, M.M.; Perovic, S. Alternative explanations of the Cosmic Microwave Background: A historical and an epistemological perspective. *Stud. Hist. Philos. Mod. Phys.* **2018**, *62*, 1–18. [[CrossRef](#)]
24. Amati, L.; D’Agostino, R.; Luongo, O.; Muccino, M.; Tantalò, M. Addressing the circularity problem in the  $E_p - E_{ISO}$  correlation of gamma-ray bursts. *Mon. Not. R. Astron. Soc. Lett.* **2019**, *486*, L46–L51. [[CrossRef](#)]
25. Einstein, A.; Rosen, N. The Particle Problem in the General Theory of Relativity. *Phys. Rev.* **1935**, *48*, 73–77. [[CrossRef](#)]
26. Morris, M.S.; Thorne, K.S. Wormholes in spacetime and their use for interstellar travel: A tool for teaching general relativity. *Am. J. Phys.* **1988**, *56*, 395–412. [[CrossRef](#)]
27. Morris, M.S.; Thorne, K.S.; Yurtsever, U. Wormholes, time machines, and the weak energy condition. *Phys. Rev. Lett.* **1988**, *61*, 1446–1449. [[CrossRef](#)]
28. Einstein, A.; Podolsky, B.; Rosen, N. Can quantum-mechanical description of physical reality be considered complete? *Phys. Rev.* **1935**, *47*, 777–780. [[CrossRef](#)]
29. Tamburini, F.; Licata, I. General relativistic wormhole connections from Planck-scales and the ER = EPR conjecture. *Entropy* **2020**, *22*, 3. [[CrossRef](#)]
30. Einstein, A. *The Born-Einstein Letters: Correspondence between Albert Einstein and Max and Hedwig Born from 1916–1955, with Commentaries by Max Born*; Walker & Company Publ.: New York, NY, USA, 1971; p. 158.
31. Misner, C.; Wheeler, J.A. Classical physics as geometry. *Ann. Phys.* **1957**, *2*, 525–603. [[CrossRef](#)]
32. Scolnic, D.; Brout, D.; Carr, A.; Riess, A.G.; Davis, T.M.; Dwomoh, A.; Jones, D.O.; Ali, N.; Charvu, P.; Chen, R.; et al. The Pantheon+ Analysis: The Full Dataset and Light-Curve Release. *Astrophys. J.* **2022**, *938*, 113. [[CrossRef](#)]
33. Brout, D.; Scolnic, D.; Popovic, B.; Riess, A.G.; Carr, A.; Zuntz, J.; Kessler, R.; Davis, T.M.; Hinton, S.; Jones, D.; et al. The Pantheon+ Analysis: Cosmological Constraints. *Astrophys. J.* **2022**, *938*, 110. [[CrossRef](#)]
34. Riess, A.G.; Yuan, W.; Macri, L.M.; Scolnic, D.; Brout, D.; Casertano, S.; Jones, D.O.; Murakami, Y.; An, G.S.; Breuval, L.; et al. A comprehensive measurement of the local value of the Hubble constant with 1 km/s/Mpc uncertainty from the Hubble Space Telescope and the SH0ES team. *Astrophys. J.* **2022**, *934*, L7. [[CrossRef](#)]
35. Harris, A. *cosmoFns* Functions for cosmological distances, times, luminosities, etc. *R J.* **2012**, *4*, 90.
36. Cash, W. Parameter estimation in astronomy through application of likelihood ratio. *Astrophys. J.* **1979**, *228*, 939–947. [[CrossRef](#)]
37. López-Corredoira, M.; Calvo-Torel, J.L. Fitting of supernovae without dark energy. *Int. J. Mod. Phys. D* **2022**, *31*, 2250104. [[CrossRef](#)]
38. Scolnic, D.M.; Jones, D.O.; Rest, A.; Pan, Y.C.; Chornock, R.; Foley, R.J.; Huber, M.E.; Kessler, R.; Narayan, G.; Riess, A.G.; et al. The complete light-curve sample of spectroscopically confirmed SNe Ia from Pan-STARRS1 and cosmological constraints from the combined Pantheon sample. *Astrophys. J.* **2018**, *859*, 101. [[CrossRef](#)]
39. Civano, F.; Eggleston, L.; Elvis, M.; Fabbiano, G.; Gilli, R.; Marconi, A.; Paolillo, M.; Piedipalumbo, E.; Salvestrini, F.; Signorini, M.; et al. Quasars as standard candles. *A&A* **2020**, *642*, A150.
40. Raikov, A.; Lovyagin, N.; Yershov, V. Superluminous quasars and mesolensing. In *Astronomy at the Epoch of Multimessenger Studies. VAK-2021 Proceedings*; Cherepashchuk, A.M., Emelyanov, N.V., Fedorova, A.A., Gayazov, I.S., Ipatov, A.V., Ivanchik, A.V., Malkov, O.Y., Obridko, V.N., Rastorguev, A.S., Samus, N.N., et al., Eds.; Janus-K Publ.: Moscow, Russia, 2022; pp. 392–394.
41. López-Corredoira, M. Pending Problems in QSOs. *Int. J. Astron. Astrophys.* **2011**, *1*, 73–82. [[CrossRef](#)]
42. Khadka, N.; Ratra, B. Do quasar X-ray and UV flux measurements provide a useful test of cosmological models? *Mon. Not. Roy. Astron. Soc.* **2022**, *510*, 2753–2772. [[CrossRef](#)]
43. Eddington, A.S. *Internal Constitution of the Stars*; Cambridge University Press: Cambridge, UK, 1926; p. 407.
44. Nernst, W. Weitere prüfung der annahme lines stationären zustandes im weltall. *Z. Phys.* **1937**, *106*, 633–661. [[CrossRef](#)]
45. Gamow, G. The expanding universe and the origin of galaxies. *Kgl. Dan. Vidensk. Selsk. Mat. Fys. Medd.* **1953**, *27*, 3–15.
46. Baryshev, Y.V.; Raikov, A.A.; Tron, A.A. Microwave background radiation and cosmological large numbers. *Astron. Astroph. Trans.* **1996**, *10*, 135–138. [[CrossRef](#)]
47. Muller, S.; Beelen, A.; Black, J.H.; Curran, S.J.; Horellou, C.; Aalto, S.; Combes, F.; Guélin, M.; Henkel, C. A precise and accurate determination of the cosmic microwave background temperature at  $z = 0.89$ . *Astron. Astrophys.* **2013**, *551*, A109. [[CrossRef](#)]

48. Luzzi, G.; Shimon, M.; Lamagna, L.; Rephaeli, Y.; De Petris, M.; Conte, A.; De Gregori, S.; Battistelli, E.S. Redshift dependence of the cosmic microwave background temperature from Sunyaev-Zeldovich measurements. *Astron. J.* **2009**, *705*, 1122–1128. [[CrossRef](#)]
49. Salvaterra, R.; Ferrara, A. Is primordial  $^4\text{He}$  truly from the Big Bang? *Mon. Not. R. Astron. Soc.* **2003**, *340*, L17–L20. [[CrossRef](#)]
50. Pagel, B.E.J. Abundances of elements of cosmological interest. *Philos. Trans. R. Soc. Lond. A* **1982**, *307*, 19–35.
51. Spite, F.; Spite, M. Abundances of Lithium in unevolved halo stars and old disk stars: Interpretations and consequences. *Astron. Astrophys.* **1982**, *115*, 357–366.
52. Reeves, H.; Fowler, W.A.; Hoyle, F. Galactic cosmic ray origin of Li, Be and B in stars. *Nature* **1970**, *226*, 727–729. [[CrossRef](#)]
53. Austin, S.M. The creation of the light elements—Cosmic rays and cosmology. *Prog. Part. Nucl. Phys.* **1981**, *7*, 1–46. [[CrossRef](#)]
54. Silverberg, R.; Tsao, C.H. Spallation processes and nuclear interaction products of cosmic rays. *Phys. Rep.* **1990**, *191*, 351–408. [[CrossRef](#)]
55. Olive, K.A.; Schramm, D.N. Astrophysical  $^7\text{Li}$  as a product of Big Bang nucleosynthesis and galactic cosmic-ray spallation. *Nature* **1992**, *360*, 439–442. [[CrossRef](#)]
56. Yamanaka, M.; Jittoh, T.; Kazunori Kohri, K.; Koike, M.; Sato, J.; Sugai, K.; Yazaki, K. Big-bang nucleosynthesis with a long-lived CHAMP including He4 spallation process. *J. Phys. Conf. Ser.* **2014**, *485*, 012020. [[CrossRef](#)]
57. Meyer, B.S.; Woosley, S.E.; Hoffman, R.D.; Mathews, G.J.; Wilson, J.R. Neutrino spallation reactions on  $^4\text{He}$  and the r-process. *AIP Conf. Proc.* **1995**, *327*, 441–445.
58. Oliver, B.M.; James, M.R.; Garner, F.A.; Maloy, S.A. Helium and hydrogen generation in pure metals irradiated with high-energy protons and spallation neutrons in LANSCE. *J. Nucl. Mat.* **2002**, *307–311*, 1471–1477. [[CrossRef](#)]
59. Abbott, B.P. et al. (LIGO, Virgo and other collaborations). Multi-messenger Observations of a Binary Neutron Star Merger. *Astrophys. J.* **2017**, *848*, L12. [[CrossRef](#)]
60. Gompertz, B.P.; Ravasio, M.E.; Nicholl, M.; Levan, A.J.; Metzger, B.D.; Oates, S.R.; Lamb, G.P.; Fong, W.F.; Malesani, D.B.; Rastinejad, J.C.; et al. The case for a minute-long merger-driven gamma-ray burst from fast-cooling synchrotron emission. *Nat. Astron.* **2022**, *7*, 67–79. [[CrossRef](#)]
61. Eddington, A.S. On the instability of Einstein's spherical world. *Mon. Not. R. Astron. Soc.* **1930**, *90*, 668–678. [[CrossRef](#)]
62. Rosen, N. Static universe and cosmic field. *Ann. Math. Pure Appl.* **1970**, *14*, 305–308. [[CrossRef](#)]
63. Sargent, W.L.W.; Searle, L. The interpretation of the helium weakness in halo stars. *Astrophys. J.* **1967**, *150*, L33–L37. [[CrossRef](#)]
64. Terlevich, E.; Terlevich, R.; Skillman, E.; Stepanian, J.; Lipovetskii, V. The extremely low He abundance of SBS:0335-052. In *Elements and the Cosmos*; Edmunds, M.G., Terlevich, R., Eds.; Cambridge University Press: Cambridge, UK, 2010; pp. 21–27.
65. Izotov, Y.I.; Thuan, T.X. The primordial abundance of  $^4\text{He}$ : Evidence for non-standard Big Bang nucleosynthesis. *Astrophys. J.* **2010**, *710*, L67–L71. [[CrossRef](#)]
66. Di Valentino, E.; Melchiorri, A.; Silk, J. Planck evidence for a closed Universe and a possible crisis for cosmology. *Nat. Astron.* **2020**, *4*, 196–203. [[CrossRef](#)]
67. Durk, J.; Clifton, T. A quasi-static approach to structure formation in black hole universes. *J. Cosmol. Astropart. Phys.* **2017**, *10*, 12. [[CrossRef](#)]
68. Yershov, V.N.; Orlov, V.V.; Raikov, A.A. Correlation of supernova redshifts with temperature fluctuations of the cosmic microwave background. *Mon. Not. R. Astron. Soc.* **2012**, *423*, 2147–2152. [[CrossRef](#)]
69. Yershov, V.N.; Orlov, V.V.; Raikov, A.A. Possible signature of distant foreground in the Planck data. *Mon. Not. R. Astron. Soc.* **2014**, *445*, 2440–2445. [[CrossRef](#)]
70. Yershov, V.N.; Raikov, A.A.; Lovyagin, N.Y.; Kuin, N.P.M.; Popova, E.A. Distant foreground and the Planck-derived Hubble constant. *Mon. Not. R. Astron. Soc.* **2020**, *492*, 5052–5056. [[CrossRef](#)]
71. Mylläri, A.A.; Raikov, A.A.; Orlov, V.V.; Tarakanov, P.A.; Yershov, V.N.; Yezhkov, M.Y. Fractality of isotherms of the Cosmic Microwave Background based on data from the Planck spacecraft. *Astrophysics* **2016**, *59*, 31–37. [[CrossRef](#)]
72. Coleman, P.H.; Pietronero, L. The fractal structure of the universe. *Phys. Rep.* **1992**, *213*, 311–389. [[CrossRef](#)]
73. Gaiete, J. The fractal geometry of the cosmic web and its formation. *Adv. Astron.* **2019**, *2019*, 6587138. [[CrossRef](#)]
74. Teles, S.; Lopes, A.R.; Ribeiro, M.B. Galaxy distributions as fractal systems. *Eur. Phys. J. C* **2021**, *82*, 896. [[CrossRef](#)]
75. Granett, B.R.; Neyrinck, M.C.; Szapudi, I. An imprint of superstructures on the microwave background due to the integrated Sachs-Wolfe effect. *Astrophys. J.* **2008**, *683*, L99–L102. [[CrossRef](#)]
76. Cai, Y.-C.; Neyrinck, M.C.; Szapudi, I.; Cole, S.; Frenk, C.S. A possible cold imprint of voids on the microwave background radiation. *Astrophys. J.* **2014**, *786*, 110. [[CrossRef](#)]
77. Kovács, A.; García-Bellido, J. Cosmic troublemakers: The Cold Spot, the Eridanus supervoid, and the Great Walls. *Mon. Not. R. Astron. Soc.* **2016**, *462*, 1882–1893. [[CrossRef](#)]
78. Kovács, A.; Jeffrey, N.; Gatti, M.; Chang, C.; Whiteway, L.; Hamaus, N.; Lahav, O.; Pollina, G.; Bacon, D.; Kacprzak, T.; et al. The DES view of the Eridanus supervoid and the CMB cold spot. *Mon. Not. R. Astron. Soc.* **2021**, *510*, 216–229. [[CrossRef](#)]

79. Labbé, I.; van Dokkum, P.; Nelson, E.; Bezanson, R.; Suess, K.A.; Leja, J.; Brammer, G.; Whitaker, K.; Mathews, E.; Stefanon, M.; et al. A population of red candidate massive galaxies  $\sim 600$  Myr after the Big Bang. *Nature* **2023**, *616*, 266–269. [[CrossRef](#)]
80. Yan, H.; Ma, Z.; Ling, C.; Cheng, C.; Huang, J.-S. First batch of  $z \approx 11$ –20 candidate objects revealed by the James Webb Space Telescope early release observations on SMACS 0723-73. *Astrophys. J. Lett.* **2023**, *942*, L9. [[CrossRef](#)]

**Disclaimer/Publisher’s Note:** The statements, opinions and data contained in all publications are solely those of the individual author(s) and contributor(s) and not of MDPI and/or the editor(s). MDPI and/or the editor(s) disclaim responsibility for any injury to people or property resulting from any ideas, methods, instructions or products referred to in the content.